Guanter, L., Segl, K., Sang, B., Alonso, L., Kaufmann, H., Moreno, J. (2009): Scene-based spectral calibration assessment of high spectral resolution imaging spectrometers. - Optics Express, 17, 14, 11594-11606

DOI: 10.1364/OE.17.011594

Scene-based spectral calibration assessment of high spectral resolution imaging spectrometers

Luis Guanter[1,*], Karl Segl[1], Bernhard Sang[2], Luis Alonso[3], Hermann Kaufmann[1] and Jose Moreno[3]

[1]*Helmholtz Centre Potsdam GFZ German Research Centre For Geosciences, Telegrafenberg, D-14473, Potsdam, Germany*

[2]*Kayser-Threde GmbH, Wolfratshauser Str. 48, D-81379, Munich, Germany*

[3]*Imaging Processing Laboratory, University of Valencia, Dr Moliner 50, 46100, Burjassot-Valencia, Spain*

**Corresponding author:*
luisguan@gfz-potsdam.de

Abstract: An accurate knowledge of the spectral calibration of imaging spectrometers is required for optimum data processing and interpretation. The scene-based spectral characterization of imaging spectrometers is frequently necessary to update or replace the pre-flight laboratory-based spectral characterization supplied by the data provider. An automatic method for the estimation of spectral calibration parameters (channel position and bandwidth) at atmospheric absorption regions from high spectral resolution imaging spectrometers (spectral sampling interval below 5 nm) is presented in this contribution. The method has been tested on two commercial instruments with spectral sampling intervals below 2.5 nm. Optical aberrations such as smile, spectrometer shift and rotation and degradation of channel bandwidth have been detected and are discussed in terms of potential error sources at the instrument level.

OCIS codes: (120.0280) Remote sensing and sensors; (010.1285) Atmospheric correction; (110.4234) Multispectral and hyperspectral imaging; (120.6200) Spectrometers and spectroscopic instrumentation

References and links

1. J. Nieke, D. Schläpfer, F. Dell'Endice, J. Brazile, and K. I. Itten, "Uniformity of imaging spectrometry data products," IEEE Trans. Geosci. Remote Sens. **46**, 3326–3336 (2008).
2. Y. Feng and Y. Xiang, "Mitigation of spectral mis-registration effects in imaging spectrometers via cubic spline interpolation," Opt. Express **16**, 15,366–15,374 (2008).
3. F. Dell'Endice, J. Nieke, D. Schläpfer, and K. I. Itten, "Scene-based method for spatial misregistration detection in hyperspectral imagery," Appl. Opt. **46**, 28032816 (2007).
4. L. Guanter, V. Estellés, and J. Moreno, "Spectral calibration and atmospheric correction of ultra-fine spectral and spatial resolution remote sensing data. Application to CASI-1500 data." Remote Sens. Environ. **109**, 54–65 (2007).
5. P. Mouroulis, R. O. Green, and T. G. Chrien, "Design of pushbroom imaging spectrometers for optimum recovery of spectroscopic and spatial information," Appl. Opt. **39**, 2210–2220 (2000).

#111005 - $15.00 USD Received 5 May 2009; revised 2 Jun 2009; accepted 3 Jun 2009; published 25 Jun 2009

6. R. O. Green, "Spectral calibration requirement for Earth–looking imaging spectrometers in the solar–reflected spectrum," Appl. Opt. **37**, 683–690 (1998).
7. S. Delwart, R. Preusker, L. Bourg, R. Santer, D. Ramon, and J. Fischer, "MERIS in-flight spectral calibration," Int. J. Remote Sens. **28**, 479–496 (2007).
8. L. Guanter, R. Richter, and J. Moreno, "Spectral calibration of hyperspectral imagery using atmospheric absorption features," Appl. Opt. **45**, 2360–2370 (2006).
9. B.-C. Gao, M. J. Montes, and C. O. Davis, "Refinement of wavelength calibrations of hyperspectral imaging data using a spectrum-matching technique," Remote Sens. Environ. **90**, 424–433 (2004).
10. R. O. Green, B. E. Pavri, and T. G. Chrien, "On-orbit radiometric and spectral calibration characteristics of EO-1 Hyperion derived with an underflight of AVIRIS and in situ measurements at Salar de Arizaro, Argentina," IEEE Trans. Geosci. Remote Sens. **41**, 1194–1203 (2003).
11. R. A. Neville, L. Sun, and K. Staenz, "Spectral calibration of imaging spectrometers by atmospheric absorption feature matching," Can. J. Remote Sens. **34**, S29–S42 (2008).
12. J. Brazile, R. A. Neville, K. Staenz, D. Schläpfer, L. Sun, and K. I. Itten, "Toward scene-based retrieval of spectral response functions for hyperspectral imagers using Fraunhofer features," Can. J. Remote Sens. **34**, S43–S58 (2008).
13. SEN2FLEX Campaign: http://www.uv.es/leo/sen2flex/
14. CEFLES-2 Campaign: http://www.fz-juelich.de/icg/icg-3/cefles/

1. Introduction

Hyperspectral applications in optical Earth Observation exploit the high spectral sampling of spaceborne and airborne imaging spectrometers to infer information from the surface and atmosphere. The quality of the hyperspectral data cube is to a large extent defined by the data uniformity in the spectral and spatial dimensions [1]. Singular defects such as dead and bad pixels, linear defects as striping and missing lines, instrument defocus and spectrometer rotations or shifts in the spatial and spectral directions of the focal plane array are sources of data nonuniformity at the instrument level. If these effects can not be minimized by instrument design, sophisticated algorithms must be developed for their detection and correction during higher-level processing [2, 3, 4].

Many recent hyperspectral applications rely on the evaluation of fine absorption features caused by surface and atmospheric constituents. Accurate knowledge of the instrument spectral performance, including spectral nonuniformity characterization, is required for the optimum algorithm development and data processing. In the spectral domain, spectrometer shifts and rotations, smile (also known as spectral line curvature) and band broadening are the most important nonuniformity sources [5]. They act modifying in different ways the shape of the spectral response functions (SRFs), the channel spectral position and the bandwidth, with respect to a given laboratory calibration: spectrometer shifts generate a spectrally-independent offset in the array of channel center wavelengths; spectrometer rotation and smile cause a variation of channel center wavelengths along the spatial dimension of the detector array, linear in the case of rotations and non-linear in the case of smile; band broadenings change the SRF with respect to laboratory calibration, normally as an increase of the full-width at half-maximum (FWHM) when the origin is an instrument defocus. Two examples of instrument nonuniformity are depicted in Fig. 1. In presence of these effects, errors will appear after data processing when the nominal spectral calibration is assumed. The magnitude of those errors depends strongly on the instrument spectral resolution and the spectral variability of the input signal, the worst situation in the real case being found when sharp atmospheric absorption features are registered by high spectral resolution instruments. For example, errors in radiance of up to 25% were reported in [6] for spectral shifts of 1 nm and bandwidths of 10 nm around water vapor absorption features.

The strong impact of spectral calibration at wavelengths affected by atmospheric absorptions has been widely exploited for scene-based spectral characterization [7, 8, 9, 10, 11, 12]. The basic approach in those methods is to search for the spectral shift of the nominal channel position providing the best fit of modelled data to one or several atmospheric absorption features. The

#111005 - $15.00 USD Received 5 May 2009; revised 2 Jun 2009; accepted 3 Jun 2009; published 25 Jun 2009

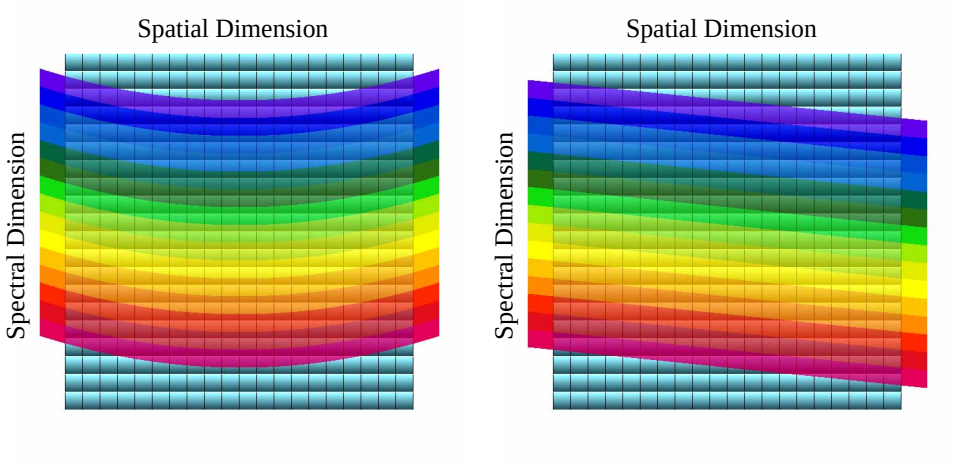

(a) Smile (b) Rotation

Fig. 1. Schematic view of instrument spectral nonuniformity. The light-blue grid depicts the detector array. Errors in pixel center wavelength along the instrument spatial dimension due to either (a) smile or (b) detector array rotation are shown.

repetition of this procedure for all samples in the across-track direction is then used to characterize potential smile and spectrometer rotation effects. A reliable characterization of spectral smile using atmospheric absorption features, while assuming a known SRF and FWHM, has been reported in [7, 8, 9]. The inversion of bandwidth changes together with spectral channel position for each across-track sample is also attempted in [10, 11], although the relatively broad spectral resolution of about 10 nm to which the methodology was applied was too coarse to derive clear trends. Preliminary analysis on the feasibility to derive SRFs in addition to spectral channel position and width are presented in [12] using modelled data of different imaging spectrometers.

A scene-based spectral characterization method using atmospheric absorption features to retrieve information on the spectral uniformity (spectrometer shift and rotation, smile and band-broadening) of high spectral resolution imaging spectrometers, considered to be those with spectral sampling interval (SSI) below 5 nm, is presented in this paper. The methodology is tested on data acquired by two commercial imaging spectrometers, the Compact Airborne Spectrographic Imager (CASI) 1500 (Itres Research Ltd., Canada) and Hyper-SIM.GA (Galileo Avionica a Finmeccanica Company, Italy), with SSIs and bandwidths of about 2 nm. These very high spectral resolution data enable the identification of clear trends in smile and across-track channel broadening as well as their interpretation at the instrument level. Exemplary results of different optical aberrations were found for the two instruments.

2. Methodology

The technique presented in this paper is an evolution of that described in [8]. That former method has been extended in order to retrieve channel FWHM in addition to center wavelength in a single inversion step. This is considered a major improvement in the case of high spectral resolution instruments. High spectral resolution data provide a proper sampling of atmospheric absorption features for the inversion of both spectral channel position and bandwidth. This might not be possible for coarser resolutions (i.e. 5-10 nm resolution instruments), as the num-

#111005 - $15.00 USD Received 5 May 2009; revised 2 Jun 2009; accepted 3 Jun 2009; published 25 Jun 2009

ber of spectral bands sampling the absorption feature may be insufficient for the inversion of two parameters; however, for the same reason the effect of not updating the nominal FWHM would not have a strong impact on this type of data.

The proposed idea is to calculate the spectral channel position and width that would produce the smoothest surface reflectance spectra when those parameters are applied to the spectral convolution of the atmospheric parameters needed in surface reflectance retrieval from at-sensor radiance. This is based on the fact that surface reflectance from natural targets is expected to be smooth, while errors in surface reflectance will appear as spikes and dips after atmospheric correction around atmospheric absorption features when a small spectral shift or band broadening would occur. A 2–D optimization procedure is used to calculate the channel position and bandwidth leading to the smoothest reflectance spectrum. In order to achieve the best sensitivity, reflectance smoothness is only evaluated around pre-defined spectral regions. In the visible and near-infrared (VNIR) spectral range, the oxygen-A absorption centered at 760 nm (O_2-A) is selected, as it is less variable in temporal and spatial terms than water vapor absorptions. The water vapor absorption feature around 1140 nm has been selected for instruments having a separate spectrometer covering the shortwave infrared (SWIR) region between 1000 and 2500 nm.

We assume that the instrument spectral characterization derived from one single spectral position is representative of the entire spectral range covered by the spectrometer. This is in principle true for spectrometer shifts, but may not be so for non-linear optical aberrations. For example, the smile effect in one edge of the spectrometer spectral domain could be slightly different to that at the other edge. In this case, smile should be characterized at a set of wavelengths and then extended to the entire spectral range by a given instrument spectral dispersion law available from laboratory measurements [7]. However, due to the fact that such a relationship is not available for most of the instruments, and that the use of different absorption features could cause errors in the smile estimation comparable to band-to-band smile differences (expected to be small), the smile calculated at one single wavelength, in which the highest accuracy is expected, is assumed here to describe the complete spectral range covered by the spectrometer.

The first step is to calculate an average at-sensor radiance spectrum from all the land pixels (cloud and water pixels are excluded) in a given along-track line. This provides a representative sampling of the sensor performance in the across-track direction with a minimum of noise and background reflectance contribution. Spectral calibration is then assessed sequentially for each across-track position. For each across-track spectrum, the procedure starts with the derivation of surface reflectance from the measured at-sensor radiance L_{sens}. If a Lambertian target is assumed, surface reflectance at spectral channel i, $\rho_{s,i}$, can be obtained by the analytical inversion of

$$L_{\text{sens},i} = L_{0,i} + \frac{1}{\pi}\frac{\rho_{s,i}(E_{\text{dir},i}\mu_{\text{il}} + E_{\text{dif},i})T_{\uparrow,i}}{1 - S_i\rho_{s,i}} \tag{1}$$

where $L_{\text{sens},i}$ is the spectral at-sensor radiance, $L_{0,i}$ is the atmospheric path radiance; μ_{il} is the cosine of the illumination zenith angle, measured between the solar ray and the surface normal; $E_{\text{dir},i}\mu_{\text{il}}$ and $E_{\text{dif},i}$ are the direct and diffuse fluxes arriving at the surface, respectively; S_i is the atmospheric spherical albedo, reflectance of the atmosphere for isotropic light entering it from the surface; $T_{\uparrow,i}$ is the total atmospheric transmittance (for diffuse plus direct radiation) in the observation direction.

The atmospheric parameters $\{L_0, E_{\text{dir}}, E_{\text{dif}}, T_{\uparrow}, S\}$ are generated by MODTRAN4 for a given set of input illumination angle, aerosol optical thickness, columnar water vapor and surface elevation. The across-track scan angle dependence in airborne sensors is considered by polynominal interpolation from a set of pre-calculated view angles. The hyperspectral output from MODTRAN4 is convolved with the instrument nominal spectral configuration, given by a triplet of

#111005 - $15.00 USD Received 5 May 2009; revised 2 Jun 2009; accepted 3 Jun 2009; published 25 Jun 2009

SRF shape, channel spectral position and bandwidth supplied by the data provider from laboratory calibration. After atmospheric correction with the nominal spectral calibration, the resulting ρ_s spectrum is likely to present artifacts in the vicinity of atmospheric absorption bands if spectral shift and broadening exist. To have a reference for the calculation of spectral shift (δ_1) and band broadening (δ_2), this reflectance spectrum is smoothed using a low-pass filter and interpolation at absorption features. The smoothed reflectance spectrum is taken as a reference in the calculation of δ_1 and δ_2 by means of an optimization procedure. The Merit Function χ^2 to be minimised is

$$\chi^2(\delta_1,\delta_2)=\sum_{i=n_1}^{n_2}\left[\rho_{s,i}(\delta_1,\delta_2)-\rho_{s,i}^{\mathrm{sm}}\right]^2, \tag{2}$$

where $\rho_{s,i}(\delta_1,\delta_2)$ is the surface reflectance in channel i from a spectral shift δ_1 and a channel broadening δ_2, $\rho_{s,i}^{\mathrm{sm}}$ is the reference smooth reflectance, and n_1,n_2 are the channel numbers at both edges of the selected spectral range, which are 750 and 775 nm in the case of the O_2-A absorption feature. Spectral response functions $SRF_i(\lambda;\delta_1,\delta_2)$ are simulated using Gaussian functions as the best approach to SRF shapes in real imaging spectrometers,

$$SRF_i(\lambda;\delta_1,\delta_2)=\exp\left[-\left(\frac{\lambda-(\lambda_{c,i}+\delta_1)}{C(f_i+\delta_2)}\right)^2\right], \tag{3}$$

where $\lambda_{c,i}$ is the nominal center wavelength of channel i, $C=(4\ln 2)^{-1/2}$, and f_i is the nominal FWHM of channel i. The final output of the inversion is the value of (δ_1,δ_2) that provides the smoothest surface reflectance spectrum. This procedure is applied sequentially to all the pixels in the across-track direction to characterize the instrument smile and across-track broadening. The instrument SRF is assumed to be Gaussian in the general case, but it could be changed to other functions when different shapes are expected, like in the case of sensors with band-binning. Given the fact that instrumental noise can be relatively large for high spectral resolution instruments and that only a reduced number of channels is available around atmospheric absorptions, no attempt to retrieve SRFs in addition to channel position and width is performed. For the reason, the resulting δ_1,δ_2 must be understood as referred to a Gaussian SRF. The assumption of a default Gaussian SRF has proven to be sufficient for the removal of reflectance errors around atmospheric absorption features.

3. Results

3.1. Data available

The proposed methodology has been tested on CASI-1500 and Hyper-SIM.GA (Hyper hereinafter) commercial imaging spectrometers. Data were acquired during the SEN2FLEX [13] (Sentinel-2 and Fluorescence Experiment) and the CEFLES2 [14] (CarboEurope, FLEX and Sentinel-2) field campaigns supported by the European Space Agency. Both campaigns were focused on activities related to both fluorescence experiments for observation of solar-induced vegetation fluorescence signal and GMES (Global Monitoring for Environment and Security) Sentinel-2 data simulation.

The SEN2FLEX campaign was held in the Barrax study site (La Mancha, Spain, 39.05°N, 2.09°W) during two phases, in June and July 2005. The area is characterized by a flat morphology and large, uniform land-use units, which make it very suitable for remote sensing calibration and validation activities. Twelve lines of CASI-1500 were acquired at an altitude of about 2000 m above ground level. CASI works in the VNIR spectral range (from 370 to 1050 nm) with a high spectral resolution mode consisting of 288 channels with bandwidths of 2.3 nm and Field Of View (FOV) equal to 23.6°. The instrument operation, the radiometric calibration and

#111005 - $15.00 USD Received 5 May 2009; revised 2 Jun 2009; accepted 3 Jun 2009; published 25 Jun 2009

the geometric correction were performed by Itres Research Ltd., Calgary, Canada. The nominal ground sampling distance was 3 m per pixel. The laboratory peak signal-to-noise ratio (SNR) is 800:1.

On the other hand, The CEFLES2 campaign was held in 2007 in South-West France in three different phases (April, June and September). The focus of CEFLES2 activites was on the agricultural area of Marmande (44.55°N, 0.16°E). This site comprises large fields of winter wheat, maize and rapeseed at three separate locations on flat land in the Garonne valley bottom. The Hyper imaging spectrometer was flown over the Marmande site during the three campaign phases. Hyper is a pushbroom sensor with VNIR and SWIR imaging capabilitites at very high spectral resolution. It samples the 400-2450 nm spectral region with two different spectrometers, one covering the VNIR (400-1000 nm) and the other covering the SWIR (1000-2450 nm). The VNIR spectrometer has 512 spectral bands with a mean spectral sampling of 1.2 nm, 1024 spatial pixels and a FOV of 41.4°. The SWIR spectrometer has 256 spectral bands, with a sampling of 5.8 nm, 320 spatial pixels and a FOV of 24.1°. Hyper operates at 2753 m above ground level. A summary of CASI and Hyper specifications is presented in Table 1.

Table 1. Specifications of SEN2FLEX/CASI and CEFLES/Hyper imaging spectrometers.

	CASI-1500	**Hyper (VNIR)**	**Hyper (SWIR)**
Imaging principle	Pushbroom-grating	Pushbroom-prism	Pushbroom-prism
Spectral range	370-1050 nm	400-1000 nm	1000-2450 nm
Spectral sampling	2.3 nm	∼1.2 nm	∼5.8 nm
Spectral resolution	2.3 nm	∼1-2 nm	∼7-9 nm
# Spectral samples	288	512	256
# Spatial samples	863	1024	320
Digital resolution	12 bits	12 bits	14 bits
Field-of-View	23.6°	41.4°	24.1°
GSD@H=1000m	1.2 m	0.7 m	1.3 m

3.2. CASI and Hyper spectral calibration assessment

Results from the spectral characterization of 2 CASI flight lines acquired during SEN2FLEX June and July campaigns are presented in Fig. 2. The calculated smile and across-track band broadening at 760 nm are displayed. Concerning smile, a clear “frown” pattern (inverted smile) is shown in Figs. 2(a) and 2(b). The change in the instrument spectral performance from the June campaign to the July campaign is detected. A systematic spectral shift of 1 nm (measured from the center of the across-track direction) and a peak-to-peak difference in channel position of about 0.9 nm is found in the June data. The asymmetry of the channel position curves would indicate the misalignment (e.g. rotation) between the instrument slit and the detector array. Different numbers are found in the July data, from which a shift of about 0.4 nm and a smile curve tilted with respect to June are visible. The same peak-to-peak smile of 0.9 nm is calculated, which is expected because it is an intrinsic characteristic of the instrument spectral dispersion. Changes in spectrometer shift and shape of the smile curve are explained by a different spectral configuration in the July campaign, as confirmed by the different set of nominal channel positions provided by the instrument operator. The smile curves in Fig. 2 are similar to those obtained in [4] from the same data when no inversion of channel bandwidth was performed together with spectral channel position. This fact supports the good decoupling between the two spectral characterization parameters in the inversion process.

#111005 - $15.00 USD Received 5 May 2009; revised 2 Jun 2009; accepted 3 Jun 2009; published 25 Jun 2009

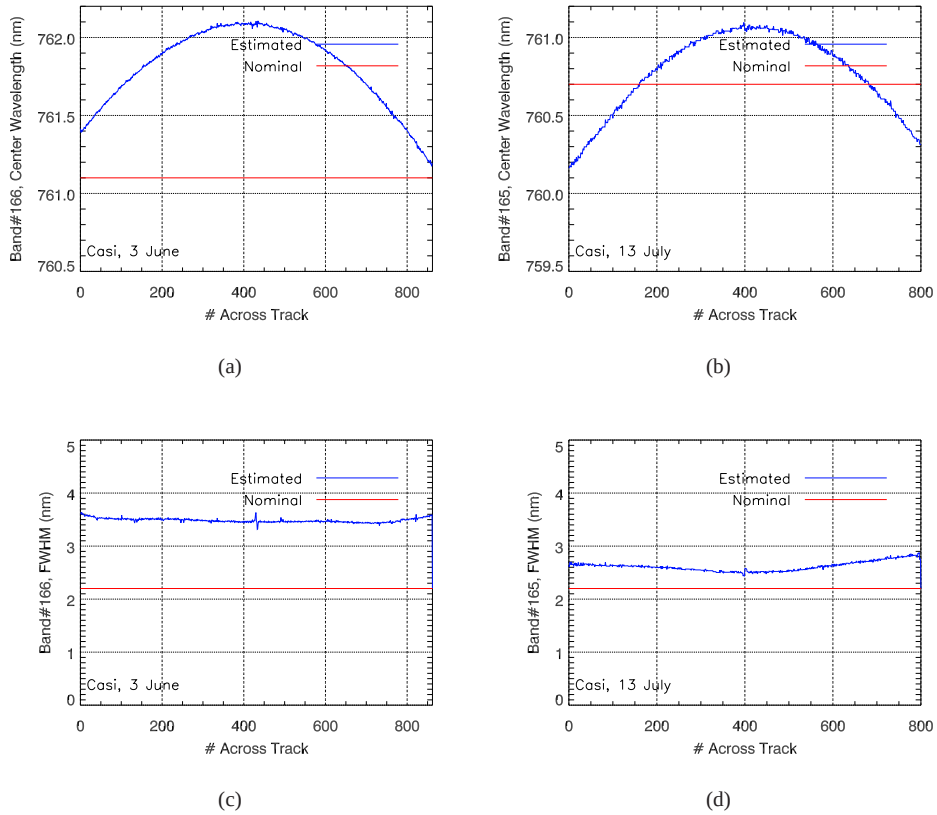

Fig. 2. CASI smile and spectral resolution characterization at O_2-A from SEN2FLEX June and July data.

The estimated CASI FWHM at O_2-A is displayed in Figs. 2(c) and 2(d). Again, the results from the June campaign differ slightly from the curve derived from July data. The estimated channel broadening from the nominal calibration is about 1 nm. A small dependence on across-track position is found, apart from a slight increase of the broadening towards the edges of the across-track direction. This could be due to the correlation between channel position and width in the retrieval methodology, or to residual atmospheric effects happening in the across-track direction due to the longer atmospheric path.

Results from the Hyper-VNIR spectral calibration assessment for the three CEFLES2 campaigns are plotted in Fig. 3. Spectrometer shift and smile at the O_2-A spectral region are displayed in the upper row, and channel broadening in the lower row. Channel position varies almost linearly along the across-track direction instead of following the bowl shape normally associated with smile. This could be explained by a misalignment (rotation, through shock or vibration) of the spectrometer with respect to the detector array, as plotted in Fig. 1(b), rather than from intrinsic instrument smile. The spectrometer shift calculated from the center of the across-track direccion varies from 1.5 to 2 nm within the three campaigns. The peak-to-peak variation of channel position also varies, from a minimum about 0.5 nm in September to a maximum of about 1 nm in April and June.

#111005 - $15.00 USD Received 5 May 2009; revised 2 Jun 2009; accepted 3 Jun 2009; published 25 Jun 2009

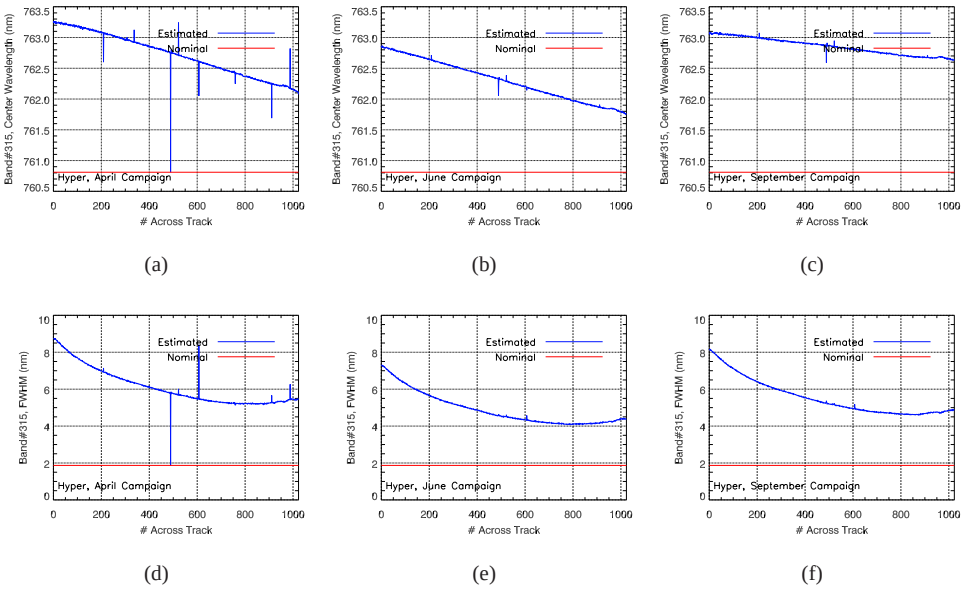

Fig. 3. Hyper-VNIR smile and spectral resolution characterization at O_2-A from CEFLES2 April, June and September campaigns.

On the other hand, a large column-dependent channel broadening is found in Hyper-VNIR. FWHM values ranging from 8.5 to 4 nm within the across-track direction have been estimated, while the nominal FWHM at the O_2-A region is 1.9 nm. Band broadening of about +1 nm were also found in CASI data by the same methodology, while the difference between nominal and estimated bandwidth in Hyper ranges from +3 to + 6 nm. It can be admitted that some systematic FWHM overestimation can be associated to the implemented methodology in view of CASI and Hyper results, but a $>$3 nm value seems beyond this assumption. In any case, the large variation of spectral resolution along the spectrometer spatial direction found by the scene-based spectral characterization method can hardly be associated to methodologic errors, as every column is processed independently. The main explanation could be the instrument defocus due to the lack of temperature and pressure control in Hyper during operations. In the absence of temperature and pressure control, as is the case for the Hyper instrument flown in CEFLES2, the laboratory-based spectral characterization would not to be representative of the real instrument performance. In addition, a possible tilt between the image of the slit and the detector array, together with a field curvature aberration, could explain the variation of the FWHM in the across-track direction. This would cause the defocus of the instrument to be more prominent in one side of the spatial direction than in the other.

Spectral characterization results from Hyper-SWIR June and September data are displayed in Fig. 4. April data were not processed because of problems of the SWIR spectrometer during the April campaign. The water vapor absorption feature at 1136 nm was used for the analysis. No apparent smile is found in the Hyper-SWIR spectrometer, but a large spectral shift of about 5 nm is found in the September data. No systematic bias in the instrument bandwidth is detected in Hyper-SWIR, even though a peak-to-peak variation of the FWHM within the spatial direction of about +4 nm is calculated.

#111005 - $15.00 USD Received 5 May 2009; revised 2 Jun 2009; accepted 3 Jun 2009; published 25 Jun 2009

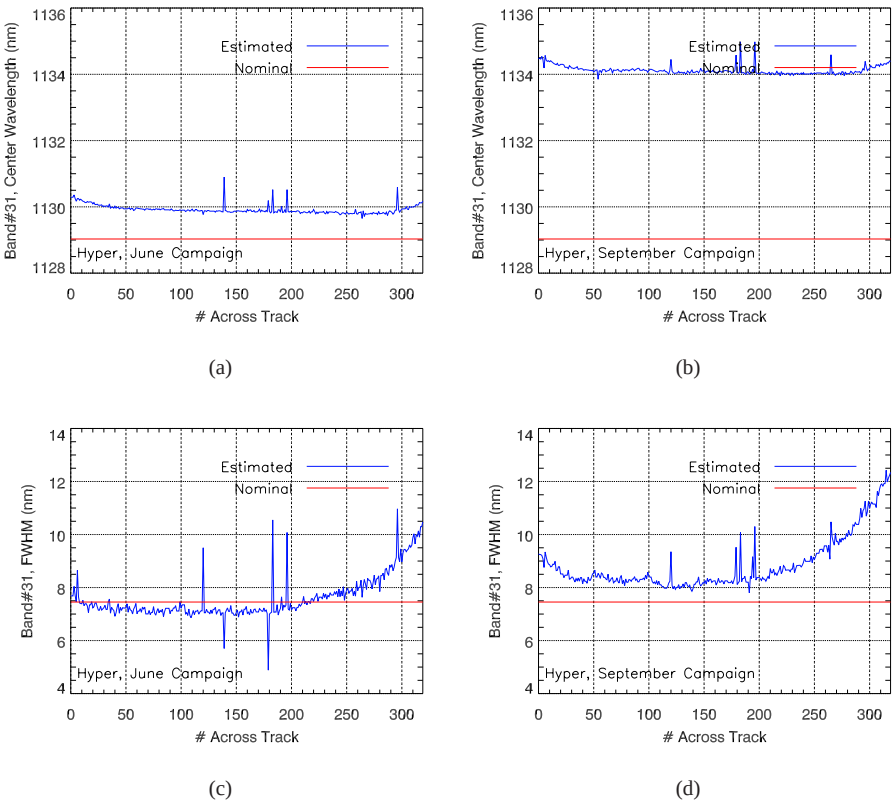

Fig. 4. Hyper-SWIR smile and spectral resolution characterization at the water vapor absorption at 1140 nm from CEFLES2 June and September campaigns.

3.3. Validation of Hyper-VNIR spectral characterization

The unexpected deviation between Hyper-VNIR nominal and estimated spectral calibration parameters has been a subject of further analysis. First, a direct comparison with CASI has been performed. As shown in Table 1, the Hyper-VNIR nominal spectral configuration is comparable to that of the SEN2FLEX 2005 CASI spectral configuration. The Hyper-VNIR has a mean spectral sampling of 1.2 nm and a nominal spectral resolution of 1-2 nm. CASI nominal spectral sampling interval and FWHM are about 2.3 nm. At-sensor radiance acquired by both spectrometers over green vegetation and bare soil surfaces are displayed in Fig. 5. The Hyper green vegetation spectrum has been extracted from the left hand side of the spatial dimension of a June line, where the estimated FWHM was about 7 nm, while the bare soil corresponds to a column around the center of the array, with a estimated FWHM of 4.2 nm. The estimated FWHM of CASI data in June was almost constant around 3.4 nm, as shown in Fig. 2. Those values are confirmed by the similar spectral resolution of different absorption features along the spectrum found in the bare soil targets, while a clearly different resolution is observed in the vegetation spectra despite the better spectral sampling interval in Hyper. A considerably better SNR is also observed in CASI data, confirming a-priori laboratory peak SNR measurements of 800:1 for CASI and 300:1 for Hyper.

The effect of updated spectral calibration parameters on CASI and Hyper-retrieved surface

#111005 - $15.00 USD Received 5 May 2009; revised 2 Jun 2009; accepted 3 Jun 2009; published 25 Jun 2009

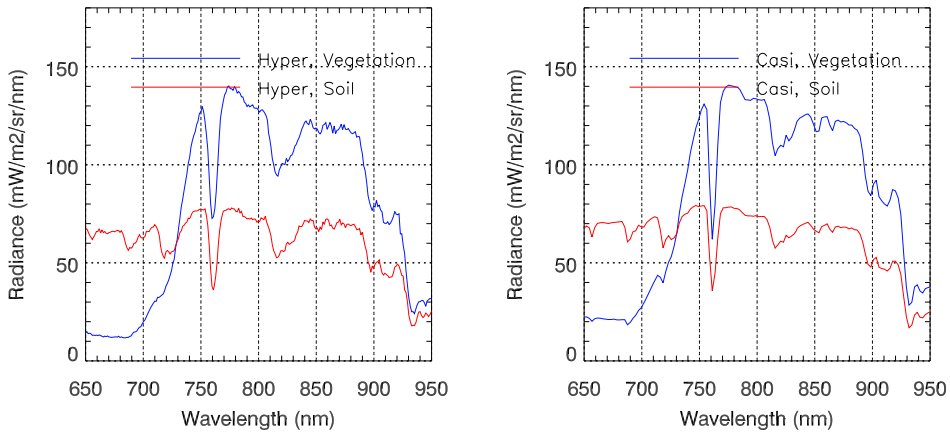

(a) (b)

Fig. 5. Comparison between Hyper-VNIR and CASI at-sensor radiance spectra acquired over green vegetation and bare soil surfaces.

reflectance between 550 and 800 nm can be seen in Fig. 6. Reflectance retrieved using the nominal spectral calibration in atmospheric correction is compared to reflectance derived using the updated channel position and width. The removal of reflectance errors around the O_2-A band after updating the spectral calibration, which is the basis of the methodology presented in this work, can be observed. Remaining small spikes may be due to unbalanced small water vapor absorption features (a default water vapor value was used to calculate the atmospheric parameters in Eq. 1), to radiometric calibration errors, or to band-to-band differences in channel position and bandwidth from O_2-A to other spectral regions were atmospheric absorptions occur. The large deviation between laboratory and estimated Hyper-VNIR spectral characterization parameters is confirmed by the reflectance errors obtained when the laboratory calibration is applied to the atmospheric correction. The oscillating reflectance patterns in Hyper in the 600-700 nm range are explained by radiometric calibration errors in the original at-sensor radiance data.

A comparison of two green vegetation pixels as measured by Hyper-VNIR at both edges of the instrument across-track direction is displayed in Fig. 7. Two targets with comparable spectral response have been selected for the sake of the comparison. The different resolution of atmospheric absorption features in the two spectra can clearly be observed, especially at the O_2-A absorption. A very different depth of this absorption is detected at both edges of the spectrometer spatial dimension. The two targets are separated by only some hundred meters and are located at the same elevation, so the only plausible explanation for such a different resolution of the O_2-A feature is due to differences in the instrument spectral performance within the spatial dimension. Without giving an idea of the real resolution value, this plot confirms the large across-track dependence of Hyper-VNIR spectral resolution.

The numerical values estimated for the Hyper-VNIR spectral shift and channel broadening have been validated by means of radiative transfer simulations. At-sensor radiance data have been modelled reproducing Hyper acquisitions. *In-situ* reflectance data measured concurrently to Hyper acquisitions have been converted to at-sensor radiance by MODTRAN4 simulations. Output data at high spectral resolution are convolved to the Hyper spectral configuration using

#111005 - $15.00 USD Received 5 May 2009; revised 2 Jun 2009; accepted 3 Jun 2009; published 25 Jun 2009

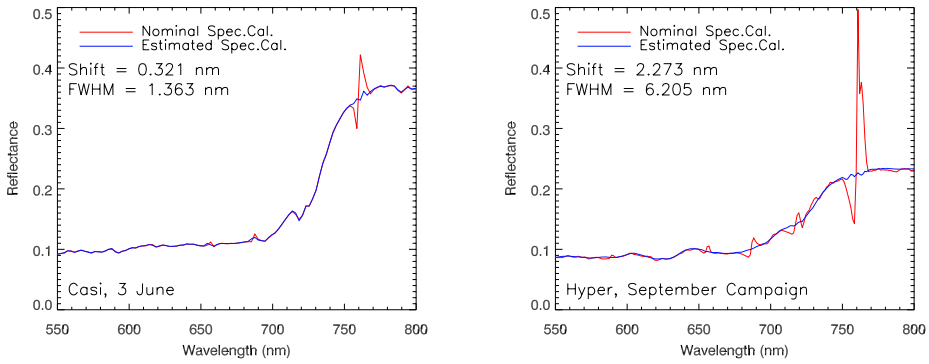

(a) (b)

Fig. 6. CASI- and Hyper-derived surface reflectance spectra between 550 and 800 nm using the nominal and the updated spectral calibration parameters during atmospheric correction. The *shift* and FWHM values in the legend correspond to the deviation of the retrieved channel position and width with respect to the nominal ones.

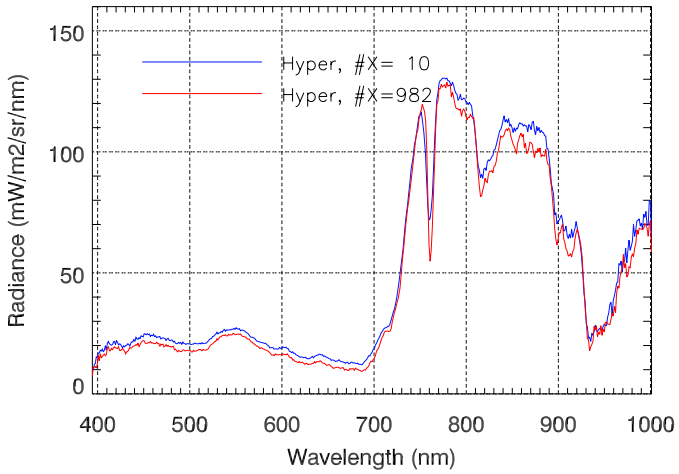

Fig. 7. At-sensor radiance from Hyper-VNIR extracted from typical green vegetation pixels at both edges of the instrument spatial dimension.

either nominal or estimated spectral calibration parameters. Simulated data are then compared to real Hyper spectra extracted from the same locations. Results are plotted in Fig. 8. The black spectra correspond to Hyper real measurements, blue spectra are the ones generated using the estimated shift and broadening, and red spectra are the ones corresponding to the simulation with the Hyper-VNIR nominal spectral configuration. It is obvious that the real spectra are closer to the simulations using the estimated calibration than to those using the nominal values. This can be seen in the different resolution of absorption features at 760, 820 or 910 nm. Ab-

#111005 - $15.00 USD Received 5 May 2009; revised 2 Jun 2009; accepted 3 Jun 2009; published 25 Jun 2009

solute radiometric calibration errors in the 600-700 nm range leading to the reflectance errors observed in Fig. 6(b) can be stated by comparison between real and simulated data.

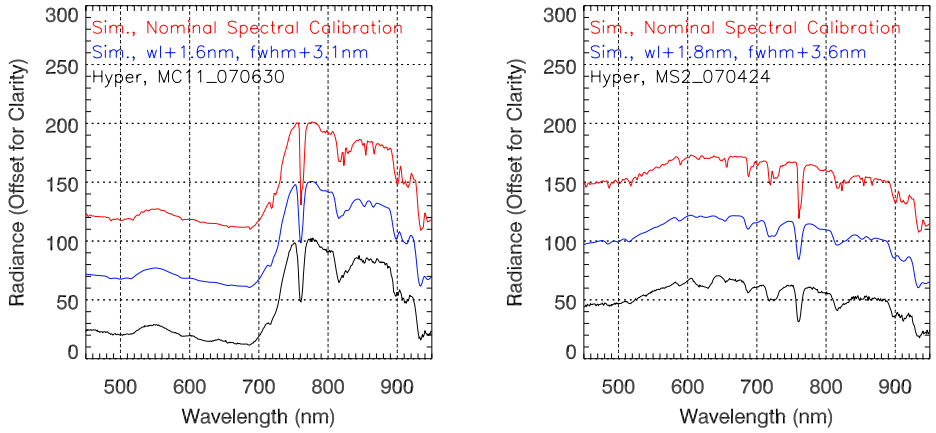

(a) (b)

Fig. 8. Comparison of Hyper-VNIR at-sensor radiance with simulated data for 2 sample targets.

4. Conclusion

A method for the scene-based spectral characterization of high spectral resolution imaging spectrometers has been presented in this paper. The method inverts spectral channel position and bandwidth, the minimization of errors in surface reflectance at atmospheric absorption regions after atmospheric correction being the criterion for the estimation of spectral calibration parameters. It has been tested on CASI-1500 and Hyper SIM.GA commercial imaging spectrometers.

The spectral calibration of the instrument is described as a combination of spectral channel position and bandwidth for a given shape of the SRF. It must be remarked that the results presented in this paper are referred to a Gaussian-like SRF. Differences between the real and the estimated spectral calibration, especially in the case of bandwidth, are expected for those instrument whose SRFs differ substantially from a Gaussian function.

The nonuniformity in the spectrometer spectral domain due to different optical aberrations, such as smile, detector array rotation or instrument defocus, has been demonstrated for both CASI and Hyper. It is expected that those optical aberrations also have an impact in the spatial domain. In particular, a shift of the pixel spatial position along the across-track direction would be associated to detector array rotations, and the degradation of the instrument point spread function would be a consequence of the instrument defocus. These effects have not been addressed in the paper due to the lack of proper data for a reliable quantitative estimation. Regular patterns and sharp borders aligned to the along- or across-track directions would be necessary for that purpose. However, the change of the Hyper spatial resolution along the spatial dimension of the VNIR spectrometer was observable by visual inspection.

The technique presented in the paper is intended to contribute to the field of optical remote sensing instrument calibration and data quality assurance, which is expected to evolve in paral-

#111005 - $15.00 USD Received 5 May 2009; revised 2 Jun 2009; accepted 3 Jun 2009; published 25 Jun 2009

lel to technical advances in coming Earth Observation instruments.

Acknowledgments

This work was supported by the projects FLEX Performance Analysis and Requirements Consolidation Study (ESA/ESTEC Contract No.21264/07/NL/FF) and EnMAP (German Federal Ministry of Economic Affairs and Technology). The authors want to thank Itres Research Ltd. (Canada) and Galileo Avionica, a Finmeccanica Company (Italy) for the data acquisition and their assistance in the interpretation of the results.

#111005 - $15.00 USD Received 5 May 2009; revised 2 Jun 2009; accepted 3 Jun 2009; published 25 Jun 2009